Transp Porous Med (2009) 78:77–99
DOI 10.1007/s11242-008-9287-8

2-D Simulation of Non-isothermal Fate and Transport of a Drip-applied Fumigant in Plastic-mulched Soil Beds. I. Model Development and Performance Investigation

Wonsook Ha · Robert S. Mansell · Dilip Shinde · Nam-Ho Kim · Husein A. Ajwa · Craig D. Stanley

Received: 2 March 2007 / Accepted: 10 September 2008 / Published online: 30 September 2008

Abstract Pre-plant application of toxic fumigants to soil beds covered by plastic film is commonly used in agriculture to control soil-borne pathogens. Plastic mulch covers tend to physically suppress the emissive loss of gaseous fumigant to the atmosphere. When liquid fumigant metham sodium (MS) is applied in irrigation water to field soil, it is rapidly transformed to the gaseous methyl isothiocyanate (MITC). The gaseous MITC is a potential atmospheric contaminant, and any untransformed MS is a potential contaminant of underlying groundwater due to the high water solubility of MS. A finite element numerical model was developed to investigate two-dimensional MITC fate/transport under non-isothermal soil conditions. Directional solar heating on soil beds, coupled heat and water flow in the soil, and non-isothermal chemical transport were included in the model. Field soil data for MITC distribution, soil water content, meteorological data, and laboratory data were used to verify the model for soil beds covered with plastic mulch. Four possible scenarios were considered: low and high drip-irrigation rates and low and high water contents. The movement of the center of MITC mass in the soil profile was effectively simulated. The lower drip-irrigation rate of MS yielded more extensive coverage of MITC in the plastic-covered soil bed. The

W. Ha (✉)
USDA-ARS/US Salinity Laboratory, Riverside, CA 92507, USA
e-mail: Wonsook.Ha@ars.usda.gov

R. S. Mansell
Department of Soil and Water Science, University of Florida, Gainesville, FL 32611, USA

D. Shinde
Division of Marine Geology and Geophysics, Rosenstiel School of Marine & Atmospheric Science, University of Miami, Miami, FL 33124, USA

N.-H. Kim
Department of Mechanical and Aerospace Engineering, University of Florida, Gainesville, FL 32611, USA

H. A. Ajwa
Department of Plant Sciences, University of California-Davis, Salinas, CA 93905, USA

C. D. Stanley
University of Florida-Gulf Coast Research and Education Center, Wimauma, FL 33598, USA

lower soil air contents due to higher soil water contents for the higher irrigation rate resulted in high concentrations of soil MITC. NRMSE (normalized root mean square error) calculations further verified that the model predicted fumigant fate/transport well under these non-isothermal field conditions.

Keywords Soil fumigant · Metham sodium (MS) · Methyl isothiocyanate(MITC) · Non-isothermal pesticide fate/transport · Numerical model

1 Introduction

Soil fumigants are used to control crop disease, kill soil-borne pests such as fungi and nematodes, and reduce population levels of nematodes in agricultural soils (Noling 1999; Duniway 2002; Cryer et al. 2003). Additional benefits include enhanced plant root health, growth, and fruit yields (Yuen et al. 1991). Drip-chemigation of fumigant provides a more effective method to allow uniform distribution in soil and to reduce atmospheric emissive loss than the conventional shank injection method (Ajwa et al. 2002).

Plastic film tends to decrease volatilization (emission) loss of fumigants from soil beds. Water-soluble fumigants are drip-applied in irrigation water to plastic-mulched soil beds in California, Florida, and Hawaii for strawberries, tomatoes, peppers, etc. (McNiesh et al. 1985; Schneider et al. 1992; Kasperbauer 2000; Noling and Gilreath 2002). Limited information is available regarding the fate and transport of such drip-chemigated soil fumigants (Papiernik et al. 2004). Fate/transport phenomena of soil fumigants are characteristically dynamic and complicated in film-covered soil beds where non-isothermal conditions are the norm. The influence of soil factors upon the formation of fumigant residues is not fully understood (Guo et al. 2003a). In addition, time-dependent, direction-oriented solar irradiance combined with the complex geometry of raised plastic-mulched soil beds provide complex thermal boundary conditions for fumigant fate/transport. Spatial distributions of soil fumigant, temperature, and water content gradients under field situations tend to be both non-symmetric and transient. Numerical simulation provides a cost-effective tool to describe/predict behaviors of chemicals applied in an agricultural field. Successful prediction of chemical fate and transport allows optimal application scenarios in order to reduce the risk of groundwater and soil pollution (Guo et al. 2003b; Do Nascimento et al. 2004). Models for non-isothermal fate and transport of chemicals for a single dimension have been investigated intensively by a few researchers (Cohen et al. 1988; Nassar and Horton 1999; Reichman et al. 2000). However, two-dimensional numerical models for non-isothermal soil fumigant fate/transport in plastic-mulched soil beds with consideration of directional solar irradiance are limited.

The HWC-MODEL, a 2-D finite element numerical model for non-isothermal heat, water, and chemical transport in plastic mulched soil beds, was developed to predict the transport/fate of drip-applied fumigants in plastic-covered soil beds used in agriculture. The HWC-MODEL was assessed using data obtained under field conditions for drip-applied metham sodium (*N*-methyl dithiocarbamate or MS). MS is one of the possible pre-plant fumigant alternatives to the formerly preferred methyl bromide (MeBr) (Ristaino and Thomas 1997) under consideration. MS degrades rapidly in the soil to form the volatile chemical methyl isothiocyanate (MITC) (Duniway 2002). The low vapor pressure of 21 mmHg and Henry's constant of 0.011 for MITC may result in contamination of underlying groundwater resources (Ajwa et al. 2002). Unpublished field data (H. Ajwa) of 2-D soil temperature, soil water content, and soil MITC concentration following drip-applied MS were used in model assessment. A water flux boundary condition was used at the soil surface with the surface water flux set equal to the drip-irrigation rate during water infiltration (Vellidis and Smajstrla 1992).

2 Model Development

2.1 Governing Equations

Differential equations for coupled heat-water flow in soil were reported earlier by Philip and de Vries (1957), de Vries (1959), and Milly and Eagleson (1980). Later, Simunek and Van Genuchten (1994) reported non-isothermal contaminant transport. Modifications of these equations were used for describing fumigant fate/transport in a plastic-mulched soil bed with a drip-chemigation line beneath the plastic mulch. In addition, meteorological boundary conditions were included to address dynamic solar radiation (Shinde 1997). Energy balance equations were used to describe plastic film conditions and bare soil surface between the covered beds. Simulation of the energy balance required consideration of net solar radiation, latent heat flux on the soil surface, sensible heat flux, and soil heat flux. Solar position, solar azimuth angle, and solar zenith were calculated using published sources (Spencer 1971; Iqbal 1983; Campbell and Norman 1998). To make numerical simulation simple, reasonable, and robust, model development was based on six simplified assumptions:

(1) Soil is anisotropic and homogeneous in the soil bed.
(2) Latent heat flux on the plastic-mulched surface is negligible.
(3) The soil moisture characteristic curve is non-hysteric.
(4) Unsaturated hydraulic conductivity of the soil is isotropic.
(5) Local equilibrium for chemical transport is assumed between soil surface, aqueous, and gaseous phases.
(6) Soil chemical and thermal properties are the same within individual finite elements.

2.2 Coupled Heat and Water Flow

Soil heat transport was described by Philip and de Vries (1957) such as

$$C_{\mathrm{h}}\frac{\partial T}{\partial t}=\frac{\partial}{\partial z}\left(\lambda\frac{\partial T}{\partial z}\right)+\frac{\partial}{\partial x}\left(\lambda\frac{\partial T}{\partial x}\right)+\rho_{\mathrm{l}}L\frac{\partial}{\partial z}\left(K_{\mathrm{v}}\frac{\partial\psi}{\partial z}\right)+\rho_{\mathrm{l}}L\frac{\partial}{\partial x}\left(K_{\mathrm{v}}\frac{\partial\psi}{\partial x}\right) \tag{1}$$

where C_h is the volumetric heat capacity of soil ($\mathrm{J\,m^{-3}\,K^{-1}}$) as a function of soil temperature T (K), λ is the thermal conductivity of soil ($\mathrm{W\,m^{-1}\,K^{-1}}$), ρ_{l} is the density of liquid water ($\mathrm{kg\,m^{-3}}$), L is the latent heat of vaporization of liquid water ($\mathrm{J\,kg^{-1}}$), K_{v} is the isothermal vapor conductivity ($\mathrm{m\,s^{-1}}$), ψ is the soil water matric potential (m), t is the time, and z and x are ordinate and abscissa in Cartesian coordinate system, respectively.

Soil moisture transport was derived by Milly and Eagleson (1980) as

$$\begin{aligned}&\left[\left(1-\frac{\rho_{\mathrm{v}}}{\rho_{\mathrm{l}}}\right)\left.\frac{\partial\theta}{\partial\psi}\right|_{T}+\frac{\theta_{\mathrm{a}}}{\rho_{\mathrm{l}}}\left.\frac{\partial\rho_{\mathrm{v}}}{\partial\psi}\right|_{T}\right]\frac{\partial\psi}{\partial t}+\left[\left(1-\frac{\rho_{\mathrm{v}}}{\rho_{\mathrm{l}}}\right)\left.\frac{\partial\theta}{\partial T}\right|_{\psi}+\frac{\theta_{\mathrm{a}}}{\rho_{\mathrm{l}}}\left.\frac{\partial\rho_{\mathrm{v}}}{\partial T}\right|_{\psi}\right]\frac{\partial T}{\partial t}\\&=\nabla\cdot\left[\left(K_{\mathrm{unsat}}+D_{\psi\mathrm{v}}\right)\nabla\psi+D_{T\mathrm{v}}^{\psi}\nabla T+K_{\mathrm{unsat}}\underline{k}\right]\end{aligned} \tag{2}$$

where ρ_{v} is the density of water vapor ($\mathrm{kg\,m^{-3}}$), θ_{a} is the volumetric air content (−), K_{unsat} is the unsaturated hydraulic conductivity ($\mathrm{m\,s^{-1}}$), $D_{\psi\mathrm{v}}$ is the matric head diffusivity of vapor ($\mathrm{m\,s^{-1}}$), $D_{T\mathrm{v}}^{\psi}$ is the temperature diffusivity of vapor in $\psi-T$ system ($\mathrm{m^2\,s^{-1}\,K^{-1}}$), and $\underline{k}$ is a z-directional unit normal vector. These two partial differential equations are transformed into matrix form via Galerkin's finite element method.

2.3 Non-isothermal Fumigant Transport

Governing equations from Simunek et al. (1992) and Simunek and Van Genuchten (1994) were utilized for numerical model development of non-isothermal soil fumigant transport, which is written as

$$(\theta_L + \rho K_D + \theta_a H)\frac{\partial C}{\partial t} = \nabla \cdot [\theta_L D_L \nabla C] + \nabla \cdot \left[\theta_a D_g H \nabla C\right] - \nabla \cdot [q_m \nabla C] - \mu_L \theta_L C \quad (3)$$

where θ_L and θ_a are volumetric water and air content [L^3L^{-3}], ρ is the soil bulk density [ML^{-3}], K_D is the linear sorption coefficient of contaminant [L^3M^{-1}], H is the Henry's constant of contaminant (−), C indicates solute concentration in aqueous phase [ML^{-3}], D_L is the dispersion coefficient for liquid phase [L^2T^{-1}], D_g is the diffusion coefficient for gaseous phase [L^2T^{-1}], and μ_L is the first-order degradation rate constant for contaminant in liquid phase [T^{-1}]. The q_m represents the volumetric flux density of liquid phase [LT^{-1}], which is obtained from the amount of irrigation water per area per time. Temperature-dependent characteristics of fate and transport, for instance, adsorption, diffusion, and degradation, were included for numerical simulations shown in part 2 of these series papers (doi:10.1007/s11242-008-9256-2).

3 Energy Balance at the Soil Bed Surface and Furrow

3.1 Solar Radiation on Bare Soil (Bare Soil Surface Boundary Condition (BC))

The energy balance equation for bare soil (Van Bavel and Hillel 1976) is:

$$Rn_{ss} + L_w E + A + S = 0 \quad (4)$$

where Rn_{ss} is the net radiation at the soil surface ($W\,m^{-2}$), $L_w E$ is the latent heat flux ($W\,m^{-2}$), L_w is the latent heat of water ($J\,kg^{-1}$), E is the evaporation rate ($kg\,m^{-2}\,s^{-1}$), A is the sensible heat flux to air ($W\,m^{-2}$), and S is the soil heat flux to and from soil below the surface ($W\,m^{-2}$). Energy fluxes entering the model domain were designated as positive and exiting fluxes as negative.

Net radiation at the soil surface is obtained by:

$$Rn_{ss} = (1 - a)\,R_g + R_l - \varepsilon\sigma\,(T_s + 273.16)^4 \quad (5)$$

where R_g is the average daily total global irradiance ($W\,m^{-2}$), R_l is the longwave sky irradiance ($W\,m^{-2}$]), T_s is the surface soil temperature (°C), and a is the albedo of the soil (Van Bavel and Hillel 1976).

The latent heat flux is (Van Bavel and Hillel 1976):

$$L_w E = -L_w\left(\rho_{v,s} - \rho_{v,a}\right)/(r_v + r_s) \quad (6)$$

where $\rho_{v,s}$ is the water vapor density of the air at the soil surface ($kg\,m^{-3}$), $\rho_{v,a}$ is the water vapor density of the atmosphere at 2 m above the ground ($kg\,m^{-3}$) (Campbell 1977), r_v is the aerodynamic resistance for water vapor transport ($s\,m^{-1}$), and r_s is the surface resistance for water vapor transport ($s\,m^{-1}$).

Sensible heat flux A is:

$$A = (T_a - T_s)\,C_p/r_v \quad (7)$$

where T_a is the daily averaged air temperature at 2 m above ground (°C) and C_p is the volumetric heat capacity of air ($J\,m^{-3}\,K^{-1}$) (Wu et al. 1996).

Soil heat flux S is defined as (Wu et al. 1996)

$$S = \lambda\,(\partial T/\partial z) \tag{8}$$

where λ is the soil thermal conductivity ($W\,m^{-1}\,K^{-1}$) and $\partial T/\partial z$ is the vertical temperature gradient at the soil bed surface. Clear sky conditions without clouds were assumed for the atmospheric boundary condition for model execution.

3.2 Solar Radiation on Plastic-covered Soil (Plastic Mulch BC)

The model includes incoming short wave solar radiation which increases soil bed temperature during daytime heating, but also long wave radiation which is directed outward during nighttime cooling. The energy balance equation for a plastic-covered soil bed (Ham and Kluitenberg 1994) is:

$$Rn_m + Rn_s + H + G = 0 \tag{9}$$

where Rn_m is the net radiation on the plastic mulch ($W\,m^{-2}$)], Rn_s is the net radiation on soil surface ($W\,m^{-2}$), H is the sensible heat flux between the mulch and atmosphere ($W\,m^{-2}$), and G is the soil heat flux ($W\,m^{-2}$). Outgoing fluxes from the plastic mulch were designated to be negative and incoming fluxes positive. The energy balance equation was adjusted to account for the characteristics of the plastic film covering raised soil beds.

Net radiation for the plastic film is shown as

$$\begin{aligned} Rn_m = {} & \alpha_m Rs\left(1+\rho^*\tau_m\rho_s\right) + \varepsilon_m\varepsilon_{sky}\sigma T_{sky}^4\left(1+\rho_{ir}^*\tau_{m,ir}\left(1-\varepsilon_s\right)\right) \\ & + \rho_{ir}^*\varepsilon_m\varepsilon_s\sigma T_s^4 + \rho_{ir}^*\left(\varepsilon_m^2\sigma T_m^4\right)\left(1-\varepsilon_s\right) - 2\sigma\varepsilon_m T_m^4 \end{aligned} \tag{10}$$

where Rs is the global irradiance ($W\,m^{-2}$), T_{sky}, T_s, and T_m are the temperatures of the sky, soil, and mulch [K], respectively, ε_{sky}, ε_s, and ε_m are the emissivities (or infrared absorptances) of the sky, soil, and mulch, respectively, α_m is the shortwave absorptance of the mulch, and $\tau_{m,ir}$ is the transmittance of the mulch in the longwave spectrum. ρ_s is the shortwave reflectance of the soil (albedo), σ is the Stefan-Boltzmann constant ($W\,m^{-2}\,K^{-4}$), and the parameters ρ^* and ρ_{ir}^* are the internal reflection functions for shortwave and longwave radiations, respectively.

The net radiation of the soil, Rn_s, is:

$$Rn_s = \left(1-\rho_s\right)\tau_m\rho^* Rs + \rho_{ir}^*\varepsilon_s\left(\tau_{m,ir}\varepsilon_{sky}\sigma T_{sky}^4 + \varepsilon_m\sigma T_m^4 + \rho_{m,ir}\varepsilon_s\sigma T_s^4\right) - \varepsilon_s\sigma T_s^4 \tag{11}$$

with the latent heat flux assumed to be zero (Ham and Kluitenberg 1994).

The sensible heat flux between the mulch and atmosphere H is:

$$H = C_p\left(T_a - T_m\right)/r_v + h_i\left(T_s - T_m\right) \tag{12}$$

where C_p is the volumetric heat capacity of air ($J\,m^{-3}\,K^{-1}$), r_v is the aerodynamic resistance ($s\,m^{-1}$), and h_i is the heat transfer coefficient inside the plastic mulch ($W\,m^{-2}\,K^{-1}$) (Garzoli and Blackwell 1981; Wu et al. 1996).

The soil heat flux G is determined by:

$$G = \lambda \frac{\partial T}{\partial z} \tag{13}$$

where λ is the soil thermal conductivity ($\mathrm{W\,m^{-1}\,K^{-1}}$).

3.3 Initial Conditions (IC)

The initial conditions were set to handle transient governing equations of soil temperature (T), soil water matric potential (ψ), and contaminant concentration (C) when the time is zero as shown.

$$T = T_0\,(z, x, 0)\,;\ \psi = \psi_0\,(z, x, 0)\,;\ C = C_0\,(z, x, 0) \tag{14}$$

3.4 Boundary Conditions (BC)

Boundary conditions were provided for soil temperature T, soil water matric potential ψ, and contaminant concentration C. Boundary conditions were separated into four different components in each case (Fig. 1). For soil temperature BC, known temperature values were given at each node along plastic mulched soil surface, soil furrow, and soil bed bottom. Measured temperature data (at time = 0; initial condition for soil temperature) were utilized for soil temperature BC. Applied boundary conditions are summarized in Table 1. A FORTRAN code provided by Shinde (1997) was modified to describe atmospheric boundary conditions.

3.5 Discretization of Governing Equations

The Galerkin's finite element method (FEM) has been widely used especially for irregular or curved computational domains. Also, solutions to the solute transport equation obtained by FEM have been reported to be more accurate than those derived by the finite difference method (Istok 1989). To minimize computational costs in FEM matrix calculations, simple triangular or rectangular elements are suggested (Huyakorn et al. 1986). Triangular elements were

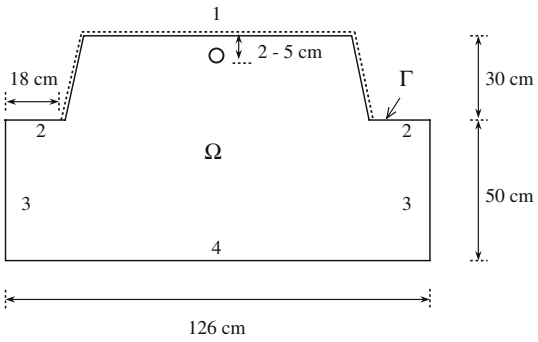

Fig. 1 Boundary conditions for coupled heat/water flow and non-isothermal fumigant transport (indicated with numbers). The Γ is delineated along the soil bed (solid line) as specified boundary conditions. The dotted line corresponds to the location of the plastic mulch. Dimensions of the soil bed domain used for model simulations in Parlier, CA (not drawn to scale), are also shown. A solid opened circle indicates the location of drip tape. The Ω represents the computational domain inside a cross-sectional view of soil bed

Table 1 Applied boundary conditions (BCs) for coupled heat/water flow and non-isothermal fumigant transport

Boundary components	Soil temperature(T) B.C.	Matric water potential (ψ) B.C.	Fumigant transport (C) B.C.
#1 (Plastic-mulched soil surface)	$T = K_1^{\mathrm{a}}$ at each node	$\frac{\partial \psi}{\partial n} = 0$	$\frac{\partial C}{\partial n} = 0$
#2 (Soil furrow)	$T = K_2^{\mathrm{a}}$ at each node	$\frac{\partial \psi}{\partial n} = -M^{\mathrm{a}}$	$\frac{\partial C}{\partial n} = -R^{\mathrm{a}}$
#3 (Sides)	$\frac{\partial T}{\partial n} = 0$	$\frac{\partial \psi}{\partial n} = 0$	$\frac{\partial C}{\partial n} = 0$
#4 (Soil bed bottom)	$T = K_3^{\mathrm{a}}$ at each node	$\psi = 0$ (Water table)	$\frac{\partial C}{\partial n} = Q^{\mathrm{a}}$

[a] Parameters

used for the HWC-MODEL. Triangular meshes were generated with GAMBIT 2.0 (mesh generation program from The Fluent® Inc., 2001). After a couple of runs with GAMBIT, an optimized mesh with 463 nodes and 842 elements was selected to reduce computational time (meshes not shown). A backward difference scheme for the finite difference method (FDM) was implemented for time domain discretization. Numerical code comprised two main submodels: coupled heat-water flow and non-isothermal soil fumigant fate and transport.

3.6 Field Measurements

Drip fumigation experiments with metham sodium (MS) were conducted on Handford sandy loam soil (coarse-loamy, mixed, thermic Typic Xerothents) at the USDA-Agricultural Research Service, Parlier, CA (Latitude: 36°35′52″ N, Longitude: 119°30′11″ W) in 2000 by H. Ajwa and colleagues. Soil bed orientation was east to west, and thus, slopes of soil bed faced north and south at the same time. Soil beds were mechanically taped with clear high density polyethylene (HDPE) film after a drip tape was applied to the soil. Dimensions for a cross section of the symmetric soil bed are shown in Fig. 1. Liquid MS was applied in irrigation water through one drip tape located at the center of the bed 2–5 cm beneath the clear plastic film. Since MS is transformed rapidly to gaseous MITC in the soil, the concentration (C) of gaseous MITC was monitored at 6, 24, 48, 96, 144, and 192 h after initial application of MS. The detection limit for MITC was 0.01 μg MITC l^{-1} air. Stainless steel soil-air sampling probes (1.0 mm, i.d.) at six depths of 0, 10, 20, 30, 40, and 60 cm were located at the bed center, 20 cm from bed center, and 40 cm from bed center.

Soil temperatures (T) were monitored every 15 min at locations where MITC sampling probes were buried in the soil bed, and the soil T data were collected using a CR-10 datalogger (Campbell Scientific, Logan, UT) to provide temporal and spatial distributions of soil T. Soil water contents were measured every 5 min using a Sentek EnviroSCAN RT6 (Australia). Average hourly one-day data of soil temperature and water content during 17–18 August 2000, were utilized to assess the coupled heat/water numerical model. The gaseous MITC distribution data were collected for 2 days during 17–18 August 2000. Averaged hourly weather data collected at Parlier, CA, from CIMIS (California Irrigation Management Information System, http://www.cimis.water.ca.gov/) were used. The weather station was located approximately 500 feet away from the study site. A brief summary of daily averages for selected weather data is provided in Table 2. Hourly average data were the smallest time increments available from CIMIS. The weather conditions during the experimental period were very dry having a low relative humidity and no rainfall.

Table 2 Selected meteorological input parameters

Parameter	Daily average	
	08/17/2000 (Julian day: 230)	08/18/2000 (Julian day: 231)
Solar radiation ($W\,m^{-2}$)	303	308
Air temperature (°C)	25.8	24.3
Vapor pressure (kPa)	1.7	1.3
Wind speed ($m\,s^{-1}$)	1.5	1.7
Wind direction (deg)	197.3	240.6
Relative humidity (%)	58	50
Dew point (°C)	14.3	10.7

3.7 Laboratory Measurements

Measurement of saturated hydraulic conductivity (K_{sat}) of field soils was accomplished using the Tempe cell technique (Sommerfeldt et al. 1984). Measurements were replicated and averaged. A soil moisture characteristic curve was obtained from the Soil Testing Lab at the University of Florida. To obtain adequate estimation of unsaturated hydraulic conductivity, empirical Eqs. 15, 16, and 17 by Van Genuchten (1980) were utilized.

$$\theta = \theta_r + \frac{(\theta_s - \theta_r)}{\left[1 + (\alpha\psi)^n\right]^m} \tag{15}$$

$$K_{unsat} = K_{sat} \frac{\left[1 - (\alpha\psi)^{n-1}\left(1 + (\alpha\psi)^n\right)^{-m}\right]^2}{\left[1 + (\alpha\psi)^n\right]^{m/2}} \tag{16}$$

$$\frac{S - S_r}{S_s - S_r} = S_e = \left[\frac{1}{1 + (\alpha\psi_w)^n}\right]^m \tag{17}$$

where θ is the volumetric soil water content, θ_r is the volumetric residual soil water content, θ_s is the volumetric saturated water content, K_{unsat} and K_{sat} are the unsaturated and saturated hydraulic conductivities, respectively, S_r is the irreducible water saturation, S_s is the fully saturated volumetric saturation, S_e is the effective saturation, ψ is the absolute value of soil matric potential, and α, n, and m are empirical parameters determined. Another empirical parameter m is related to n by the relationship:

$$m = 1 - (1/n) \tag{18}$$

A simple numerical code based on Van Genuchten's equation (1980) was validated against the soil moisture characteristic curve to evaluate Van Genuchten's model parameters, α ($\alpha = 0.015\,cm^{-1}$) and n ($n = 1.99$), which are utilized to obtain the unsaturated hydraulic conductivity of soils. The measured soil moisture characteristic curve is shown in Fig. 2. A brief summary of soil parameters is shown in Table 3. The Handford sandy loam soil from the experimental site consisted of 62% sand, 27% silt, and 11% clay. Chemical parameters for MITC are presented in Table 4.

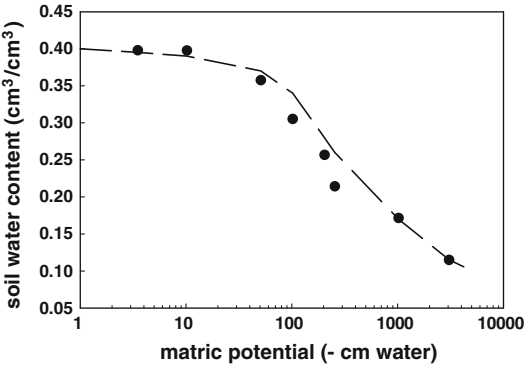

Fig. 2 Experimental soil moisture characteristic data (dotted) and obtained semi-empirical curve (dashed) for Hanford sandy loam from Parlier, CA

Table 3 Field soil parameters

Parameter	Value
Bulk density, ρ_b ($g\,cm^{-3}$)	1.55
Particle density, ρ_{pd} ($g\,cm^{-3}$)	2.54
Porosity, n_p	0.39
Saturated hydraulic conductivity, K_{sat} ($cm\,s^{-1}$)	1.41e-2
Soil organic matter (%) (weight basis)	0.42

Table 4 Chemical parameters for fumigant MITC (Methyl Isothiocyanate)

Parameter	Value
Molecular formula	$C_2\ H_3\ NS$
Molecular weight	73.1
Vapor pressure (mm Hg) (at 20°C)	21
Density ($g\,cm^{-3}$) (at 20°C)	1.21
Henry's constant (−)	0.011
Log K_{ow} (calculated)	1.37
Melting point (°C)	35–36
Boiling point (°C) (at 760 mm Hg)	118–119
Solubility in water ($g\,l^{-1}$) (at 20°C)	8.2
Sorption coefficient ($l\,kg^{-1}$) (at 20°C)	0.09
Half-life (days)	7

This table was reorganized based on data from Tomlin (2003) and unpublished data

4 Qualitative Evaluation of the HWC-MODEL for Soil Fumigant Fate/Transport

The numerical model of coupled heat/water flow and non-isothermal contaminant transport was tested against field data. First, the coupled heat/water flow submodel was tested against observed soil temperature and water content data (Ha 2006) but is not presented here. Second, the non-isothermal chemical transport submodel also focused on the drip-chemigation effect under the field condition to simulate the impact of drip-applied fumigant throughout the soil bed and was tested.

4.1 Non-isothermal Soil Fumigant MITC Transport

Gaseous MITC was measured in the field and compared with simulation results. It was assumed that direct partitioning between the vapor and solid phases was negligible when the

Table 5 Experimental scheme of drip-irrigation/fumigation treatments

Case number	Drip-irrigation rate ($l h^{-1} m^{-1}$ tape)	Equivalent water depth (mm)	Irrigated amount of water (l)	Concentration of metham sodium in water ($mg l^{-1}$)	Drip duration time (hr:min)
#1 (Low irrigation rate)	1.9	50	969	490	8:00
#2 (High irrigation rate)	7.5	50	969	490	3:00
#3 (Small water amount)	2.5	25	484	980	2:15
#4 (Large water amount)	2.5	75	1451	327	11:00

soil water content was high enough to allow soil-particle surfaces to be covered with a layer of water (Shikaze and Sudicky 1994). The mathematical model of non-isothermal chemical transport was written in terms of chemical concentration in the liquid phase. Concentration of simulated gaseous MITC was re-calculated using Henry's constant for the comparison with field data. Numerical simulation of MITC was reported only for the gaseous phase of MITC due to the availability of MITC experimental results.

Field experiments were conducted to investigate the influence of selected water irrigation rates and applied water amounts upon MITC distributions in field soil. MS concentration in applied drip-irrigation water was $490 mg l^{-1}$. The first data set described MITC distributions with respect to irrigation water rates and the second data set showed MITC distributions associated with selected applied water amounts. Major change in soil water contents stopped within 24 h after drip-irrigation/chemigation. Numerical simulations were conducted to test against all two-dimensional data for a given time. Details for the drip-irrigation treatments for the experimental setup are shown in Table 5.

4.1.1 Effect of Irrigation Rates on the Distribution of MITC

The field experiment was performed with two different irrigation rates, 1.9 and 7.5 l/h. Data were collected at 6, 24, and 48 h after initiation of drip-irrigation. Data and modeling results are presented with respect to irrigation rates and time.

4.1.2 Case 1: MITC Distribution with a Low Irrigation rate (1.9 l/h)

Case 1 consisted of a 1.9 l/h drip irrigation rate, an equivalent depth of applied water of 50 mm, and an approximate drip duration time of 8 h. Experimental and simulated MITC distributions at 6 h after onset of drip-irrigation are given in Fig. 3a, b. The highest MITC concentration was approximately $1400 \mu g l^{-1}$ air for both experiment and model simulations. Experimental MITC distributions revealed an approximately elliptical pattern with lateral extension exceeding downward extension (Fig. 3a). The numerical model appeared to overestimate downward movement of MITC as shown by the contours of lower MITC concentrations, such as 200 and $400 \mu g l^{-1}$ air (Fig. 3b). Although MITC transport was greater laterally than vertically for both simulation results and experimental data, greater vertical MS dispersion occurred for model results relative to experimental ones.

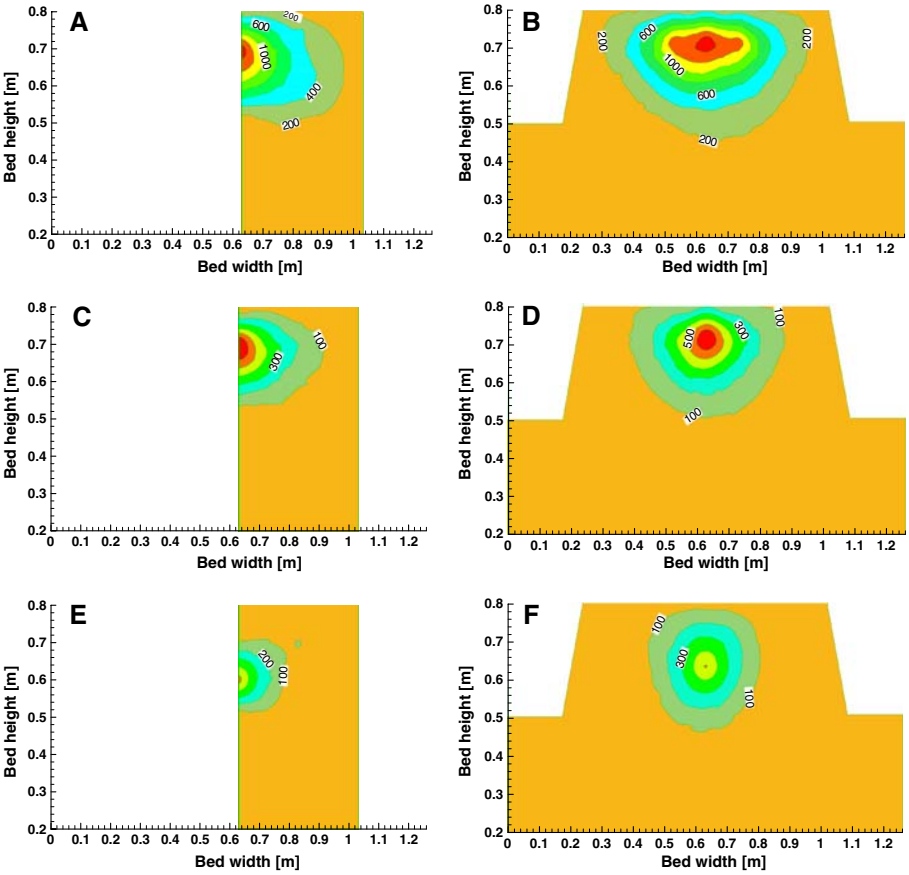

Fig. 3 The MITC distribution data at the rate of 1.9 l/h with 50 mm of irrigation water for 6 h **a**, **b** 24 h **c**, **d** and 48 h **e**, **f** after the onset of drip-irrigation. MITC concentration is presented in μg MITC l^{-1} air. **a**, **c**, **e** Measured. **b**, **d**, **f** Simulated

Simulated and experimental MITC distributions for Case 1 are reported in Figs. 3c and 4d at 24 h after onset of drip-irrigation. A center of mass for MITC was located at 0.1 m depth for both modeled and experimental data. A maximum MITC concentration of only 600 μg l^{-1} air in comparison to 1400 μg l^{-1} air 18 h earlier (Figs. 3a, b) was attributed to enhanced volatilization and degradation of MITC in the soil under conditions of lower water contents. Thus, after drip-irrigation stopped, MITC was possibly volatilized through the more available air phase as a result of drier soil water conditions. Gaseous MITC possibly had greater exposure time to soil microbes for microbial MITC degradation during that period. The relatively warm soil temperature at 24 h may also have contributed to enhanced degradation (Fig. 3b, d). MITC concentrations less than 100 μg l^{-1} air were observed from data along the surface of the soil bed. However, simulations revealed that MITC concentrations of greater than 100 μg l^{-1} air remained near the soil surface. The simulation exhibited more lateral spread of MITC than vertical transport, as was observed from the experimental data (Fig. 3c).

The Case 1 MITC distributions are given in Fig. 3e and f at 48 h after the onset of drip-irrigation. Simulations (Fig. 3f) reveal more upward MITC transport relative to experimental

results (Fig. 3e). Enhanced upward MITC movement likely resulted from increased vaporization rate of MITC at the time of the post-irrigation event (10:00 AM). Decreased area of the inner contours showing the maximum concentration of 500 μg MITC l^{-1} air (Fig. 3f) occurred for model simulation and experimental data (Fig. 3e). As time passed, maximum MITC concentrations decreased from 1400 at 6 h to 600 and 500 μg l^{-1} air at 24 and 48 h post-drip-irrigation, respectively. As the inner contour centers moved deeper into the soil, the simulations characteristically provided radially symmetric fumigant movement in all directions rather than unsymmetric movement due to enhanced lateral movement (Fig. 3b, d, f). The mulched soil surface acted as a physical barrier for upward contaminant flow during numerical model simulation. As the inner contours moved downward with time, the soil bed became less restrictive to chemical movement.

4.1.3 Case 2: MITC Distribution with a High Irrigation Rate (7.5 l/h)

The experimental setup of Case 2 consisted of 7.5 l/h drip-irrigation rate, 50 mm water depth, and approximately 3 h of drip application duration time. Measured and simulated MITC distributions for Case 2 are presented in Figs. 4a and b for 6 h after the onset of drip-irrigation.

Experimental and modeled results showed that propagation of the lowest MITC concentration contour ceased within 6 h after drip-chemigation since drip-irrigation duration time was 3 h (Figs. 4a and b). Data for Case 2 revealed that more downward direction of water infiltration occurred than Case 1 (Fig. 3a). A symmetric circular propagation of MITC isoconcentration lines occurred (Fig. 4a) rather than an elliptical pattern of lateral movement for Case 1 (Fig. 3a). The higher irrigation rate of 7.5 l/h for Case 2 generated more downward movement of MITC concentration profile, compared to a lower irrigation rate for Case 1 (1.9 l/h). Simulations were in agreement with field data (Fig. 4a, b).

The MITC distribution for Case 2 is given in Fig. 4c and d at 24 h post-irrigation. The center of maximum MITC concentration appeared to be located at 66 cm soil depth for data (Fig. 4c) and 69 cm for simulation (Fig. 4a). In contrast, the location of the highest MITC concentration contour in the simulation remained unchanged from 6 h (Fig. 4b) to 24 h (Fig. 4d) for Case 2. Data and simulation in Fig. 4c and d were uncorrelated probably because a large area of MITC still remained above the 0.5 m under the clear plastic mulch (Fig. 4c), while reduced lateral transport of MITC was observed from the simulation shown in Fig. 4d. MITC is still prohibited from spreading laterally probably due to very high soil moisture content (data not shown).

Measured and simulated MITC concentration profiles at 48 h post-irrigation for Case 2 are given in Fig. 4e and f. The peak MITC concentration was observed as 200 μg l^{-1} air for both experimental and simulated results. Greater spacing between 50 and 100 μg l^{-1} air of isoconcentration lines was observed in the simulation relative to data.

For both Cases 1 and 2, the center of the highest MITC mass moved downward from approximately 0.1–0.2 m depth within 48 h after initiation of drip-irrigation in general. The gravity effect could move the center of MS mass distribution and then MS could transform to MITC. In Case 1, the decreasing trend of highest MITC concentrations in field data and simulations was from 1400 at 6 h to 600 and 500 μg l^{-1} air at 24 and 48 h after post-irrigation, respectively, in comparison to the trend in Case 2 from 800 at 6 h to 350 and 200 μg l^{-1} air at 24 and 48 h after post-irrigation, respectively. If maximum MITC concentrations at 24 and 48 h post-drip-irrigation are compared between Cases 1 and 2 (600 vs. 350 μg MITC l^{-1} air and 500 vs. 200 μg MITC l^{-1} air) assuming that the drip-irrigation event did not affect MITC concentration results at 24 and 48 h post drip-irrigation, the drip-irrigation method of low irrigation rate yielded higher peak MITC concentration in the field. Note that the initial

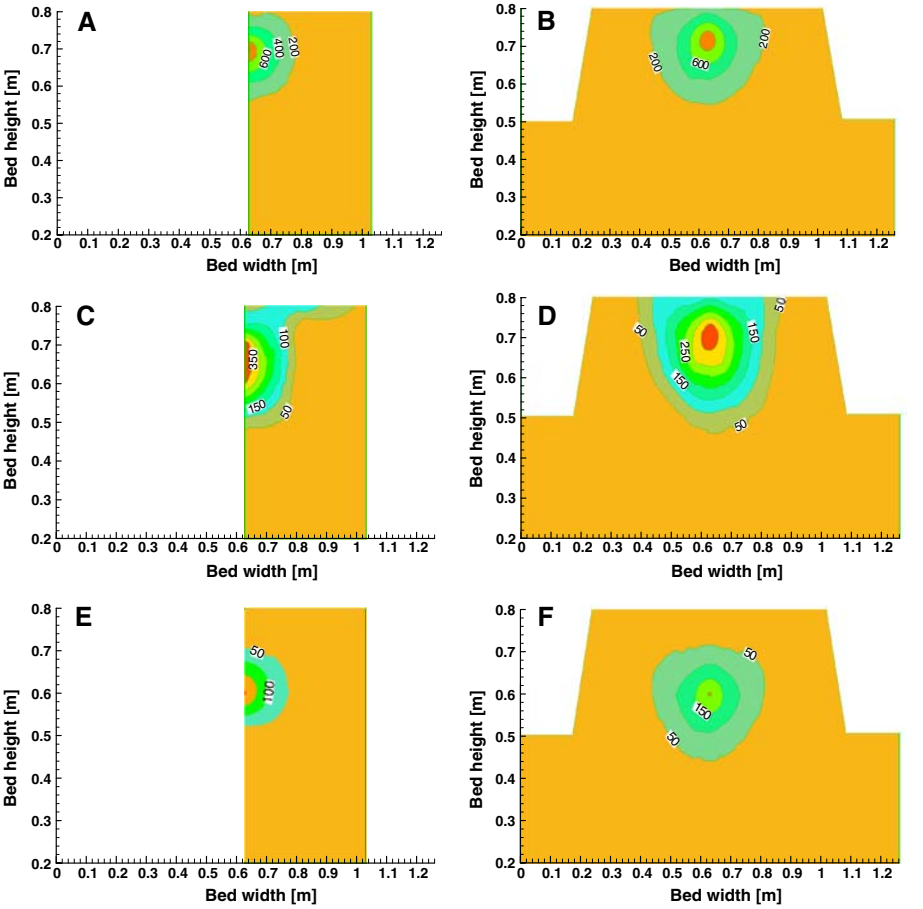

Fig. 4 The MITC distribution data at the rate of 7.5 l/h with 50 mm of irrigation water for 6 h **a**, **b** 24 h **c**, **d** and 48 h **e**, **f** after the onset of drip-irrigation. MITC concentration is presented in μg MITC l^{-1} air. **a**, **c**, **e** Measured. **b**, **d**, **f** Simulated

concentration of applied MS as a liquid phase for both cases was 490 mg l^{-1} and irrigated water amount was 50 mm of depth (approximately equal to 9691 of water) for both cases. Thus, decreased potential fumigation effect on soil pathogens for Case 2 is expected due to insufficient MITC concentration for the higher irrigation rate in the soil field. Lateral movement of MITC at 6 and 24 h post-irrigation was especially limited in the experimental data for Case 2 with the higher drip-irrigation rate. Decreased spatial coverage of MITC distribution which occurred within 0.2 m from the soil bed center may possibly be less effective so that only a limited soil bed area received soil fumigant to control soil-borne pests (personal communication with H. Ajwa).

4.2 Effect of Irrigation Water Amounts on the Distribution of MITC

An experiment was performed with two different equivalent water depths, 25 and 75 mm, for Cases 3 and 4, respectively, with a drip-irrigation rate of 2.5 l/h. Experimental data were collected at 6, 24, and 48 h after the initiation of drip-irrigation.

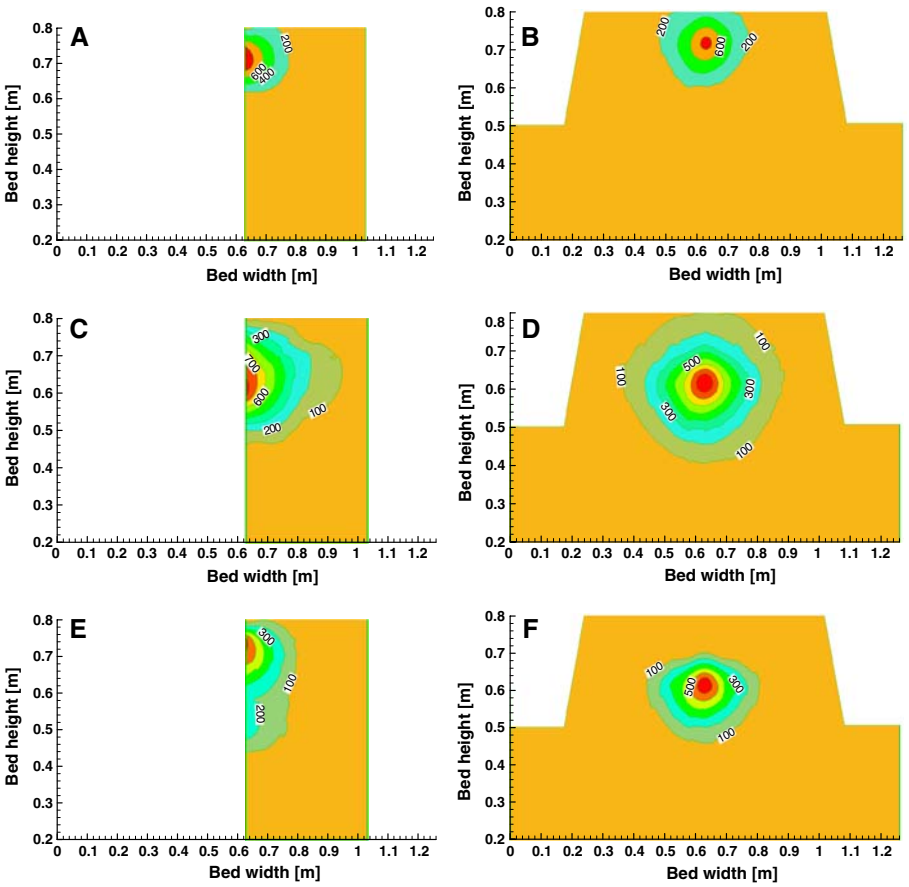

Fig. 5 The MITC distribution data at the rate of 2.5 l/h with 25 mm of irrigation water for 6 h **a**, **b** 24 h **c**, **d** and 48 h **e**, **f** after the onset of drip-irrigation. MITC concentration is presented in μg MITC l^{-1} air. **a**, **c**, **e** Measured. **b**, **d**, **f** Simulated

4.2.1 Case 3: MITC Distribution with a small irrigation water amount (25 mm)

Case 3 included a 2.5 l/h of drip-irrigation rate, 25 mm of water depth, and approximately 2 h of drip duration time. MITC distribution of observed and predicted data for Case 3 is given in Fig. 5a and b. The measured maximum concentration of 800 μg MITC l^{-1} air had a wider spatial distribution than the modeled result. This resulted due to model underestimation of MITC concentration near 0.7 m depth in the bed. Simulations were in good agreement with data. The trend of MITC movement in the experimental result showed more lateral flow of MITC than vertical flow.

Experimented and simulated MITC distributions for Case 3 at 24 h after drip-irrigation are given in Fig. 5c and d. A peak MITC concentration of 800 μg l^{-1} air did not decrease during the period of time from 6 to 24 h (Fig. 5a–d). Even though this soil bed still had the maximum MITC concentration of 800 μg l^{-1} air, the contour of 100 μg l^{-1} air apparently did not reach the edge of the soil bed laterally for observed and modeled data. The increased amount of volumetric soil air content beyond 0.2 m from center of the soil bed was observed

(personal communication from H. Ajwa). This resulted in less available MITC beyond the lateral mark of 0.83 m from center of soil bed because more air space contributed to increased vaporization and degradation of MITC (data not shown). In general, lateral movement of the MITC exceeded vertical transport in the experimental data (Fig. 5c). The numerical model did not predict a concentration range less than 300 $\mu g\,l^{-1}$ air.

The MITC distributions of measured and simulated data for Case 3 at 48 h post-irrigation are shown in Fig. 5e and f. Simulation results were not in good agreement with experimental data. The contour of maximum MITC concentration from experimental data (Fig. 5e), by contrast, revealed a center of maximum MITC concentration near 10 cm soil depth. Since most data showed relocation of peak MITC concentration observed at approximately 20 cm soil depth at 48 h, experimental results shown in Fig. 5e may possibly be in error in concentration distribution near the drip tape.

4.2.2 Case 4: MITC Distribution with a Large Irrigation Water Amount (75 mm)

Experimental conditions for Case 4 included 2.5 l/h of drip-irrigation rate, 75 mm of water depth, and approximately 11 h of drip duration time. Lateral MITC movement for Case 4 at 6 h after onset of drip-irrigation (Fig. 6a) dominated vertical movement due to the existence of more available air phase in the soil bed. Note that drip-irrigation was operative at the time of observation. The simulation provided a symmetrical or circular pattern of MITC distribution (Fig. 6b). Moreover, a larger zone of 800 μg MITC l^{-1} air in Fig. 6b indicated that simulations overestimated MITC concentrations near 70 cm soil depth at the soil bed center.

Observed data showed the upper half of the soil bed was almost covered by irrigation water in Fig. 6c. The increased amount of water possibly inhibited MITC volatilization resulting in concentrations of more than 300 μg MITC l^{-1} air being detected as a subsurface band in the soil bed. Corresponding soil water content data are not presented here. The upper half of the soil bed was almost saturated by irrigation water, generating more lateral distribution of MS in the water phase than the vertical movement of that in the soil bed. Simulations did not match well with experimental results in this case.

Observed and simulated MITC results for Case 4 indicate that the wide distribution of the highest concentrations is attributed to water saturation near 10 cm soil depth (data not shown). Numerical model results were generally in good agreement with experimental results. Although a large amount of irrigation water was applied (75 mm of water is equivalent to approximately 1450 l of water), the water irrigation method for Case 4 did not allow MITC to significantly leach the soil bed in 48 h after drip-irrigation (Fig. 6c and e).

Peak MITC concentrations remained relatively constant during 6–24 h after irrigation onset for both data in Case 3, but decreased only for simulations for Case 4. Decreased MITC concentration 24 h after the onset of drip-irrigation was expected since no additional MITC was applied through drip tape after drip-irrigation (compare Fig. 5a–d, and Fig. 6b versus d). Lower soil air contents appeared to contribute to the remaining highest MITC concentration than the amount of chemigated MS in the soil bed up to 24 h. All experimental MITC distributions reveal enhanced lateral movement relative to vertical movement except Fig. 5e. Even though the gaseous MITC concentrations were monitored in the field, approximately 90 times higher concentrations of liquid MS were expected, which also remained in the soil bed (Henry's constant of MITC is 0.011; Ajwa et al. 2002). However, a simple estimation can help us determine how high the liquid MS concentration could be measured in the soil bed. If the gaseous MITC concentration is as low as 100 $\mu g\,l^{-1}$ air, expected liquid MS

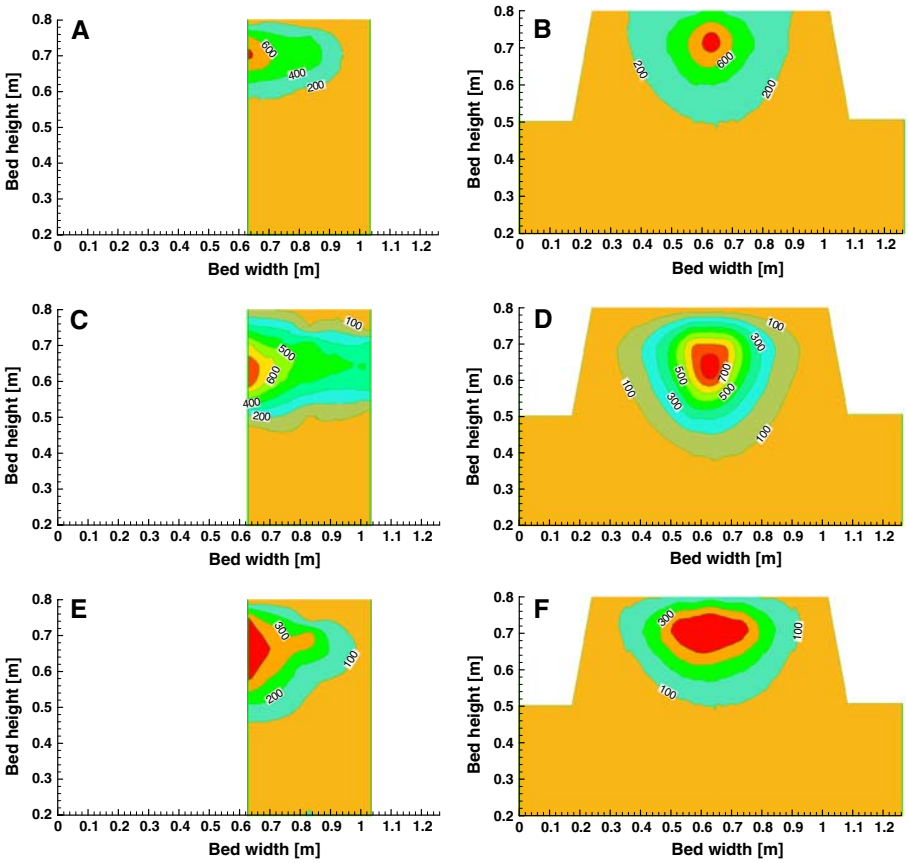

Fig. 6 The MITC distribution data at the rate of 2.5 l/h with 75 mm of irrigation water for 6 h **a**, **b** 24 h **c**, **d** and 48 h **e**, **f** after the onset of drip-irrigation. MITC concentration is presented in μg MITC l^{-1} air. **a**, **c**, **e** Measured. **b**, **d**, **f** Simulated

concentration could be at least 9090 $\mu g\,l^{-1}$ water. Because planting occurs after the MITC distribution, these lateral movement characteristics could be a benefit to plant root to control remaining soil pathogens. In conclusion, experiments with selected water amounts with fixed irrigation rate yielded helpful information for the better practice of using drip-irrigation for application of MITC.

4.3 Comparison Between Isothermal and Non-isothermal Conditions for Soil Fumigant Transport

To determine if non-isothermal soil conditions impact spatial patterns of soil fumigant distribution, model simulations were conducted under isothermal and non-isothermal soil conditions. An experimental condition utilized for numerical simulation was 1.9 l/h of drip-irrigation rate and 50 mm of the equivalent water depth (Case 1). A constant soil temperature of 26°C (average measured soil temperature on that day) was assumed for numerical simulation of isothermal contaminant transport throughout the entire soil bed with respect to adsorption, diffusion, and vaporization of MITC. In contrast, the simulation result of soil

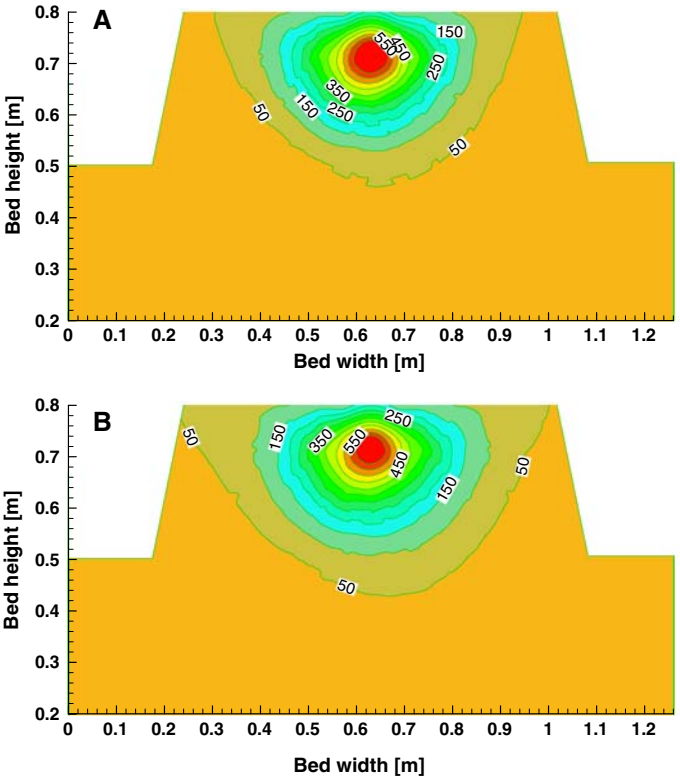

Fig. 7 Comparison of MITC distribution at the rate of 1.9 l/h with 50 mm of irrigation water for 24 h after the onset of drip-irrigation. MITC concentration is presented in μg MITC l^{-1} air. **a** Isothermal condition. **b** Non-isothermal condition

temperature for coupled heat/water flow from previous section was used for non-isothermal contaminant transport.

Simulated MITC spatial and temporal distributions under isothermal and non-isothermal contaminant transport conditions are given in Fig. 7. The simulation result in Fig. 7b is identical to Fig. 3d; however, different interpretation methods were applied to Fig. 7b. First, contours of MITC distribution were closely spaced in Fig. 7b than those in Fig. 3d. Second, minimum MITC concentrations were represented up to 50 μg MITC l^{-1} air.

A couple of findings after close investigation of Fig. 7b are summarized. First of all, the lowest MITC concentration of 50 μg l^{-1} air in the non-isothermal condition revealed much wider spatial distribution of MITC than that in the isothermal condition (7a) near the north edge of the soil bed. It appeared that non-isothermal behavior of MITC was reflected by a directional solar radiation at 10:00 AM, which resulted in heated south side (right-hand side of the soil bed) stimulating migration of MS from warm (south) to cool (north) side of the soil bed. Therefore, transformation of MS to MITC may have occurred more intently in the north than the south side of the soil bed during morning time. Apparently, non-symmetrical spatial mass distribution of MITC in the soil bed depicted the impact of directional solar radiation. This result confirmed non-isothermal behavior of MITC in a plastic-mulched soil bed. Secondly, simulation results obtained under the non-isothermal condition showed better agreement with measured data as determined by NRMSE (normalized root mean square

Table 6 Calculated NRMSE values for isothermal and non-isothermal soil conditions

Data point (m)	NRMSE	
	Measured data versus simulated data for isothermal soil conditions; Figs. 3c versus 7a	Measured data versus simulated data for non-isothermal soil conditions; Fig. 3c versus 7b
(0.63,0.75)	0.364	**0.212**
(0.63,0.7)	0.128	**0.103**
(0.63,0.6)	0.248	**0.142**
(0.83,0.75)	**0.118**	0.204
(0.83,0.7)	0.295	**0.150**
(0.83,0.6)	0.336	**0.151**
(0.83,0.5)	**0.046**	0.124

error). The MITC distribution profiles for isothermal and non-isothermal soil conditions were compared to measured field data point to point to yield NRMSE. The NRMSE values were calculated to investigate how much simulated data were in good agreement with measured data with suggested comparison criterion (Janssen and Heuberger 1995). The NRMSE is calculated from root mean square error (RMSE) divided by the average of observed values (Janssen and Heuberger 1995). The RMSE is obtained by:

$$\mathrm{RMSE} = \sqrt{\frac{\sum_{i=1}^{N} (M_i - O_i)^2}{N}} \tag{19}$$

where M_i and O_i represent the predicted (modeled) and experimental (observed) values of ith prediction and experimental result and N denotes the number of data. In this work, 0.15 of NRMSE was selected to represent a good agreement between measured and calculated data. The estimation of NRMSE for (1) measured data vs. isothermal simulation result and (2) measured data vs. non-isothermal simulation result was conducted using the simulation results of Figs. 3c and 7 and results presented in Table 6. Comparison was conducted for seven points of interest due to availability of field data.

A comparison of NRMSE calculations between isothermal and non-isothermal soil conditions revealed that modeling results for non-isothermal soil condition showed better agreement with experimental data on five selected points of (0.63,0.75), (0.63,0.7), (0.63,0.6), (0.83,0.7), and (0.83,0.6) (NRMSE in bold from the result of non-isothermal soil condition in Table 6) than those under isothermal soil condition. Most values were located within an acceptable range of NRMSE (NRMSE $\leq$ 0.15 or close to 0.15) to show good agreement with measured data except 0.212 of NRMSE at (0.63,0.75). In isothermal soil condition, only two data points showed better simulation results with field data than those in non-isothermal soil condition (NRMSE in bold from the result of isothermal soil condition in Table 6). The general trend of NRMSE values from the comparison between simulated data of a non-isothermal soil condition and measured data also gave better agreement than that for an isothermal soil condition at the rate of 2.5 l/h and 25 mm of equivalent water depth (data not shown). Although not all simulation results of MITC distribution were compared with measured data, calculation results of NRMSE gave indication that simulated data matched well with field data in general.

5 Quantitative Evaluation of the HWC-MODEL for Soil Fumigant Fate/Transport

Both qualitative and quantitative techniques of model evaluation are commonly used when model predictions are compared with experimental observations. To quantitatively define good agreement between numerical model and experimental data, Schelde et al. (1998) proposed a criterion that normalized root mean square error (NRMSE) be equal to or less than 10%. A complication, however, exists in simulation results of non-isothermal contaminant transport in terms of 2-D spatial geometry of contours compared to one-dimensional model comparison of Schelde and colleagues' work. Because of this reason, a less restrictive criterion that NMRSE is 15% or less was employed to assess the distribution of MITC in the field. Calculated RMSE and NRMSE for water irrigation rates and applied water amounts are presented in Tables 7 and 8. Selected data points were based on the availability of measuring points of field data. Estimations of RMSE and NRMSE were conducted on the data taken at 24 h after the initiation of drip-irrigation because soil water content change and MITC concentration distribution change reached near equilibrium at 24 h post drip-irrigation.

For the case with 1.9 l/h water irrigation rate and 50 mm water amount, NRMSE values near 10 and 20 cm soil depths gave good agreement between modeled and observed data (NRMSE $\leq$15.1%, shown in case 1 of Table 7). Simulations for the case with 7.5 l/h drip-

Table 7 Estimated RMSE and NRMSE for the selected data points of MITC distribution in case of selected irrigation water rates (non-isothermal conditions)

Data point (m)	RMSE	NRMSE
Case 1 (Figs. 3c and d) Experimental condition: 1.9 l/h, 50 mm water Time after the onset of drip-irrigation: 24 h		
(0.63,0.8)	N/A	N/A
(0.63,0.75)	70	0.212
(0.63,0.7)	80.01	0.103
(0.63,0.6)	47.28	0.142
(0.63,0.5)	N/A	N/A
(0.83,0.8)	N/A	N/A
(0.83,0.75)	23.72	0.204
(0.83,0.7)	30	0.150
(0.83,0.6)	17.02	0.151
(0.83,0.5)	4.76	0.124
(1.03,0.75)	N/A	N/A
(1.03,0.7)	N/A	N/A
(1.03,0.6)	N/A	N/A
(1.03,0.5)	N/A	N/A
Case 2 (Figs. 4c, d) Experimental condition: 7.5 l/h, 50 mm water Time after the onset of drip-irrigation: 24 h		
(0.63,0.8)	50.72	0.568
(0.63,0.75)	96.24	0.626
(0.63,0.7)	2.29	0.006
(0.63,0.6)	55.24	0.156
(0.63,0.5)	3.56	0.054
(0.83,0.8)	20	0.25
(0.83,0.75)	N/A	N/A
(0.83,0.7)	N/A	N/A
(0.83,0.6)	5	0.1
(0.83,0.5)	0.44	0.0099
(1.03,0.75)	1.64	0.125
(1.03,0.7)	2.39	0.175
(1.03,0.6)	N/A	N/A
(1.03,0.5)	N/A	N/A

Table 8 Estimated RMSE and NRMSE for the selected data points of MITC distribution in case of selected irrigation water amounts (non-isothermal conditions)

Data point (m)	RMSE	NRMSE
Case 3 (Figs. 5c, d) Experimental condition: 2.5 l/h, 25 mm water Time after the onset of drip-irrigation: 24 h		
(0.63,0.8)	11	0.159
(0.63,0.75)	150	0.429
(0.63,0.7)	120	0.231
(0.63,0.6)	28.65	0.034
(0.63,0.5)	60	0.25
(0.83,0.8)	2	0.25
(0.83,0.75)	10.55	0.177
(0.83,0.7)	50	0.278
(0.83,0.6)	15.3	0.078
(0.83,0.5)	10	0.125
(1.03,0.75)	7.2	0.316
(1.03,0.7)	2.5	0.111
(1.03,0.6)	3.7	0.156
(1.03,0.5)	0.55	0.124
Case 4 (Fig. 6c, d) Experimental condition: 2.5 l/h, 75 mm water Time after the onset of drip-irrigation: 24 h		
(0.63,0.8)	32.6	0.29
(0.63,0.75)	4.7	0.013
(0.63,0.7)	50	0.078
(0.63,0.6)	9.8	0.012
(0.63,0.5)	10	0.034
(0.83,0.8)	19.6	0.282
(0.83,0.75)	15	0.143
(0.83,0.7)	238.8	0.489
(0.83,0.6)	206	0.507
(0.83,0.5)	25	0.294
(1.03,0.75)	16	0.348
(1.03,0.7)	280	0.875
(1.03,0.6)	310	0.886
(1.03,0.5)	11.2	0.359

irrigation rate and 50 mm water amount were in good agreement with observed data in most cases except at (0.63,0.8) and (0.63,0.75) where poor agreement occurred (Case 2 of Table 7 based on Fig. 4d). Contours for data were centered (if MITC concentration $>150\,\mu g\,l^{-1}$ air) near 0.14 m depth (Fig. 4c). The MITC distribution of observed data had much higher concentration near the drip-irrigation tubing. Also, partial inundation of irrigation water occurred on the soil surface. As discussed earlier, the likelihood of experimental error for those points is high.

Calculated RMSE and NRMSE values are shown in Table 8 to investigate the effect of water amounts on model efficiency. The numerical model results represent MITC distribution similar to experimental data. Among 14 points of observation, only a few higher NRMSE values were reported (NRMSE ≤ 0.429). These can be explained by two possible reasons. First, lateral extension of MITC concentration contours exceeded downward extension (Fig. 5c), whereas simulation results tended to have symmetrical lateral and vertical extensions (Fig. 5d) due to assumption of uniform bulk density (homogeneous soil). Second, more spatially dispersed $100\,\mu g$ MITC l^{-1} air contour from simulation (Fig. 5d) resulted in lower concentrations than experimentally observed at (0.63,0.75), (0.63,0.7), (0.83,0.8), and (0.83,0.7) (Case 3 of Table 8).

Model results were in good agreement with experimental data along the center line of the soil bed probably due to high concentration along the center line ($x = 0.63$ m). All NRMSE

values along the center of the soil bed were <10% except the center point of soil surface at (0.63,0.8). The numerical model, however, did not accurately predict lateral transport of MITC from the center of the soil bed to the bed edge due to non-uniform packing of soil beds toward the edge. The numerical model did not seem to match experimental results which yielded significantly high NRMSE values for most data points at 20 and 40 cm (bed edge) distance from the soil bed (Case 4 of Table 8) probably resulting from low MITC concentrations. This result was mainly attributed to the fact that, in most cases, the model tended to simulate MS dispersion in a circular pattern.

6 Conclusions

A FEM numerical model of coupled heat/water flow including non-isothermal contaminant transport (HWC-MODEL) was developed with emphasis on non-isothermal characteristics of adsorption, diffusion, and degradation. The effect of a directional solar irradiation on the soil bed was included to describe unevenly heated soil bed with space and time. Non-isothermal chemical transport was tested using observed data for field experiments with liquid MS applied by drip-irrigation under film-covered soil bed. The experiments examined effects of water irrigation rates and water amounts on temporal and spatial distributions of MITC in soil beds. Simulated results were in good agreement with experimental data. Shorter duration times for irrigation generated a longer water distribution time after termination of the drip-irrigation, which is directly associated with increased probability for volatilization, diffusion, and degradation of MITC in the soil beds. For the quantitative evaluation, NMRSE < 15% revealed good agreement between simulation results and experimental data for 24 h after initiation of drip-irrigation. Model results showed NMRSE < 10% along the center line of the soil bed (except for the center point of the soil surface at (0.63,0.8)), suggesting good agreement with experimental data.

References

Ajwa, H.A., Trout, T., Mueller, J., Wilhelm, S., Nelson, S.D., Soppe, R., et al.: Application of alternative fumigants through drip irrigation systems. Phytopathology **92**(12), 1349–1355 (2002). doi:10.1094/PHYTO.2002.92.12.1349

Campbell, G.S.: An Introduction to Environmental Biophysics. Springer-Verlag, New York (1977)

Campbell, G.S., Norman, J.M.: An Introduction to Environmental Biophysics. Springer-Verlag, New York (1998)

Cohen, Y., Taghavi, H., Ryan, P.A.: Chemical volatilization in nearly dry soils under non-isothermal conditions. J. Environ. Qual. **17**(2), 198–204 (1988)

Cryer, S.A., Van Wesenbeeck, I.J., Knuteson, J.A.: Predicting regional emissions and near-field air concentrations of soil fumigants using modest numerical algorithms: a case study using 1,3-dichloropropene. J. Agric. Food Chem. **51**(11), 3401–3409 (2003). doi:10.1021/jf0262110

de Vries, D.A.: Simultaneous transfer of heat and moisture in porous media. Am. Geophys. Union Trans. **39**(5), 909–916 (1958)

Do Nascimento, N.R., Nicola, S.M.C., Rezende, M.O.O., Oliveira, T.A., Oberg, G.: Pollution by hexachlorobenzene and pentachlorophenol in the coastal plain of Sao Paulo state, Brazil. Geoderma **121**(3–4), 221–232 (2004). doi:10.1016/j.geoderma.2003.11.008

Duniway, J.M.: Status of chemical alternatives to methyl bromide for pre-plant fumigation of soil. Phytopathology **92**(12), 1337–1343 (2002) doi:10.1094/PHYTO.2002.92.12.1337

Garzoli, K.V., Blackwell, J.: An analysis of the nocturnal heat loss from a single skin plastic greenhouse. J. Agric. Eng. Res. **26**(3), 203–214 (1981). doi:10.1016/0021-8634(81)90105-0

Guo, M., Papiernik, S.K., Zheng, W., Yates, S.R.: Formation and extraction of persistent fumigant residues in soils. Environ. Sci. Technol. **37**(9), 1844–1849 (2003a). doi:10.1021/es0262535

Guo, M., Yates, S.R., Zheng, W., Papiernik, S.K.: Leaching potential of persistent soil fumigant residues. Environ. Sci. Technol. **37**(22), 5181–5185 (2003b). doi:10.1021/es0344112

Ha, W.: Non-isothermal fate and transport of drip-applied fumigants in plastic-mulched soil beds—model development and verification. Ph.D. dissertation, University of Florida, Gainesville, Florida (2006)

Ham, J.M., Kluitenberg, G.J.: Modeling the effect of mulch optical properties and mulch-soil contact resistance on soil heating under plastic mulch culture. Agric. For. Meteorol. **71**(3–4), 403–424 (1994). doi:10.1016/0168-1923(94)90022-1

Huyakorn, P.S., Jones, B.G., Andersen, P.F.: Finite element algorithms for simulating three-dimensional groundwater flow and solute transport in multiplayer systems. Water Resour. Res. **22**(3), 361–374 (1986). doi:10.1029/WR022i003p00361

Iqbal, M.: An Introduction to Solar Radiation. Academic Press, Ontario, Canada (1983)

Istok, J.: Groundwater Modeling by the Finite Element Method. American Geophysical Union, Washington D. C. (1989)

Janssen, P.H.M., Heuberger, P.S.C.: Calibration of process-oriented models. Ecol. Modell. **83**(1–2), 55–66 (1995). doi:10.1016/0304-3800(95)00084-9

Kasperbauer, M.J.: Strawberry yield over red versus black plastic mulch. Crop Sci. **40**(1), 171–174 (2000)

McNiesh, C.M., Welch, N.C., Nelson, R.D.: Trickle irrigation requirements for strawberries in coastal California. J. Am. Soc. Hortic. Sci. **110**(5), 714–718 (1985)

Milly, P.C.D., Eagleson, P.S.: The coupled transport of water and heat in a vertical soil column under atmospheric excitation. Department of Civil Engineering, Massachusetts Institute of Technology, Cambridge, Massachusetts (1980)

Nassar, I.N., Horton, R.: Transport and fate of volatile organic chemicals in unsaturated, nonisothermal, salty porous media: 1. Theoretical development. J. Hazard. Mater. **B69**, 151–167 (1999). doi:10.1016/S0304-3894(99)00099-0

Noling, J.W.: Nematode management in commercial vegetable production. Florida Cooperative Extension Service, Institute of Food and Agricultural Sciences, University of Florida, Gainesville, Florida (1999)

Noling, J.W., Gilreath, J.P.: Methyl bromide: Progress and problems identifying alternatives, vol. II. Florida Cooperative Extension Service, Institute of Food and Agricultural Sciences, University of Florida, Gainesville, Florida (2002)

Papiernik, S.K., Yates, S.R., Dungan, R.S., Lesch, S.M., Zheng, W., Guo, M.: Effect of surface tarp on emissions and distribution of drip-applied fumigants. Environ. Sci. Technol. **38**, 4254–4262 (2004). doi:10.1021/es035423q

Philip, J.R., de Vries, D.A.: Moisture movement in porous materials under temperature gradients. Am. Geophys. Union Trans. **38**(2), 222–232 (1957)

Reichman, R., Wallach, R., Mahrer, Y.: A combined soil-atmosphere model for evaluating the fate of surface-applied pesticides 1. Model development and verification. Environ. Sci. Technol. **34**(7), 1313–1320 (2000). doi:10.1021/es990356e

Ristaino, J.B., Thomas, M.W.: Agriculture, methyl bromide, and the ozone hole: can we fill the gaps? Plant Dis. **81**(9), 964–977 (1997). doi:10.1094/PDIS.1997.81.9.964

Schelde, K., Thomsen, A., Heidmann, T., Schjønning, P.: Diurnal fluctuations of water and heat flows in a bare soil. Water Resour. Res. **34**(11), 2919–2929 (1998). doi:10.1029/98WR02225

Schneider, R.C., Zhang, J., Anders, M.M., Bartholomew, D.P., Caswellchen, E.P.: Nematicide efficacy, root-growth, and fruit yield in drip-irrigated pineapple parasitized by rotylenchlus-reniformis. J. Nematol. **24**(4), 540–547 (1992)

Shikaze, S.G., Sudicky, E.A.: Simulation of dense vapor migration in discretely fractured geologic media. Water Resour. Res. **30**(7), 1993–2009 (1994). doi:10.1029/94WR00066

Shinde, D.: Modeling coupled water-heat flow and impacts upon chemical transport in mulched soil beds. Ph.D. dissertation, University of Florida, Gainesville, Florida (1997)

Simunek, J., Vogel, T., Van Genuchten, M.T.: The SWMS_2D code for simulating water flow and solute transport in 2-D variably saturated media, Ver. 1.1, Research report no. 126. U.S. Salinity Lab, USDA-ARS, Riverside, California (1992)

Simunek, J., Van Genuchten, M.T.: The CHAIN_2D code for simulating two-dimensional variably saturated water flow, heat transport and transport of solutes involved in sequential first-order decay reactions, Research report no. 136. U.S. Salinity Lab, USDA-ARS, Riverside, California (1994)

Sommerfeldt, T.G., Schaalje, G.B., Hulstein, W.: Use of tempe cell, modified to restrain swelling, for determination of hydraulic conductivity and soil water content. Can. J. Soil Sci. **64**(2), 265–272 (1984)

Spencer, J.W.: Fourier series representation of the position of the Sun. Search **2**(5), 172 (1971)

Tomlin, C.D.S. (ed.): The Pesticide Manual: A World Compendium, 13th edn. British Crop Protection council, Farnham, UK (2003)

Van Bavel, C.H.M., Hillel, D.I.: Calculating potential and actual evaporation from a bare soil surface by simulation of concurrent flow of water and heat. Agric. Meteorol. **17**, 453–476 (1976). doi:10.1016/0002-1571(76)90022-4

Van Genuchten, M.T.: A closed-form equation for predicting the hydraulic conductivity of unsaturated soils. Soil Sci. Soc. Am. J. **44**, 892–898 (1980)

Vellidis, G., Smajstrla, A.G.: Modeling soil water redistribution and extraction patterns of drip-irrigated tomatoes above a shallow water table. T. ASAE **35**(1), 183–191 (1992)

Wu, Y., Perry, K.B., Ristaino, J.B.: Estimating temperature of mulched and bare soil from meteorological data. Agric. For. Meteorol. **81**(3–4), 299–323 (1996). doi:10.1016/0168-1923(95)02320-8

Yuen, G.Y., Schroth, M.N., Weinhold, A.R., Hancock, J.G.: Effects of soil fumigation with methyl bromide and chloropicrin on root health and yield of strawberry. Plant Dis. **75**(4), 416–420 (1991)